Consequences of secondary zeolite growth on catalytic performance in DMTO studied over DDR and CHA

Yarulina, I.; Dikhtiarenko, A.; Kapteijn, F.; Gascon, J.

DOI
10.1039/c6cy02307j

Publication date
2017

Document Version
Accepted author manuscript

Published in
Catalysis Science & Technology

Journal Name

ARTICLE

Consequences of secondary zeolite growth on catalytic performance in DMTO studied over DDR and CHA

uReceived 00th January 20xx,
Accepted 00th January 20xx

DOI: 10.1039/x0xx00000x

www.rsc.org/

I.Yarulina,[a] A.Dikhtiarenko,[a] F.Kapteijn[a] and J.Gascon[a,*]

Zeolites with DDR (Sigma-1 and ZSM-58) and CHA (SSZ-13) topology were synthesized by seed assisted and direct hydrothermal synthesis in order to investigate the effects of fast crystal growth on catalytic performance. Application of small amount of seeds (0.1% wt.) significantly reduced synthesis time of all the studied zeolites. XRD and NH_3-TPD analyses did not reveal any difference in crystallinity and acidity. On the other hand, IR spectroscopy clearly demonstrates the presence of multiple defects, internal silanols (3729 cm^{-1}) and silanol nests (3400 cm^{-1}), as a result of accelerated crystal growth kinetics. Comparison of catalytic properties in the dimethyl ether to olefins (DMTO) reaction at 400°C and 450°C revealed that, despite smaller crystal sizes, zeolites prepared by secondary growth display shorter lifetimes due to faster coking rates, the latter being a result of silanols promoting hydrogen transfer reactions. This work highlights the importance of zeolite quality for catalytic application and the necessity to optimize current synthetic protocols based on secondary growth.

Introduction

Zeolites are microporous aluminosilicates widely employed in chemical industry as molecular sieves and catalysts.[1] Due to their unique properties such as ability to ion-exchange, thermal and chemical stability and shape selectivity; they are the working horses in many processes ranging from waste water treatment[2] to gas separation[3-5] and catalysis.[6, 7] Fluid catalytic cracking (FCC), hydrocracking and methanol to hydrocarbons (MTH) are among the most important industrial processes utilizing zeolites as catalysts. In all of them, the active site is a proton - Brønsted acid - counterbalancing negative charge of zeolite framework due to the insertion of Al. However, catalysis by zeolites is not limited to Brønsted acidity. For instance, similar isomorphous substitutions with tetravalent metals such as Sn- or Zr- may act as Lewis acid sites to catalyse Baeyer-Villiger reaction,[8] aldol condensation[9] and many other reactions[10] of interest.[11] Besides, zeolites can host different metals in the form of nanoparticles or as counter ions, such as in case of Cu-CHA for the selective catalytic reduction (SCR) of NOx.[12]

Given the relatively large number of known zeolite frameworks and their outstanding properties, one could easily argue that zeolites should be even more extensively used in large scale processes. However, issues associated with the high price of certain structure directing agents, large synthesis times and, in some cases, reproducibility issues, still hamper zeolite scale up.[8, 13-16]

In order to address most of these issues, the application of secondary (or seeded) growth has been proposed.[17] The idea behind this method is rather simple – certain amount of crystals of the desired topology is added to the mixture prior to hydrothermal synthesis. If the amount of crystals is big enough (10 – 25 wt.% relative to silica source) crystallization proceeds without structure-directing agent (SDA).[18] On the other hand, even negligible amount of crystals (≈ 0.1%) significantly decrease the crystallization time in the presence of an SDA. For example, Yu *et al.*[19] reported ultrafast synthesis of SAPO-34 in the presence of seeds in 10 min. The faster formation of products is attributed to the fact that addition of seeds suppresses the necessity of a nucleation step either by partial dissolution of seeds to provide growth surface for new crystals[20] or *via* a core-shell growth mechanism.[21]

Naturally, fast crystal growth might lead to the formation of some framework imperfections, which in turn can affect physical and chemical (read as catalytic) properties. Thus, the aim of this work is to compare structural and catalytic properties of zeolites obtained *via* seeded growth approach with the ones synthesized *via* direct hydrothermal synthesis. In this spirit, we synthesized a series of 8MR zeolites with two different topologies (DDR and CHA) using both methods and targeting the same morphology and acidity and assessed their catalytic properties in the Dimethyl Ether-to-Olefins reaction. DMTO (and the methanol to olefins process, MTO) is very sensitive to parameters related to quality of crystals, such as Si and Al distribution,[22] presence of defects,[23] and thus serves as an excellent probe reaction to assess even small differences in zeolite quality.

[a] *Catalysis Engineering, Chemical Engineering Department, Delft University of Techonology, Van der Maasweg 9, 2629 HZ Delft, The Netherlands.*
* j.gascon@tudelft.nl

Electronic Supplementary Information (ESI) available: [details of any supplementary information available should be included here]. See DOI: 10.1039/x0xx00000x

Table 1. Experimental details on zeolite synthesis procedure.

Sample	Zeolite	Type of growth	Seeds	Gel composition SDA:Na_2O:SiO_2 :Al_2O_3:H_2O	Time, h
D-DDR_1	Sigma-1	Direct	-	20 : 3 : 60 : 1 : 2400	144
S_1-DDR_1	Sigma-1	Seeded	BM* D-DDR_1	20 : 3 : 60 : 1 : 2400	16
S_2-DDR_1	Sigma-1	Seeded	S_1-DDR_1	20 : 3 : 60 : 1 : 2400	16
D-DDR_2	ZSM-58	Direct	-	15 : 10 : 60 : 1 : 2400	120
S-DDR_2	ZSM-58	Seeded	BM* D-DDR_2	15 : 10 : 60 : 1 : 2400	16
D_1-CHA	SSZ-13	Direct	-	20 : 10 : 100 : 1 : 4400	120
D_2-CHA	SSZ-13	Direct	-	20 : 10 : 100 : 1 : 4400	24
S_1-CHA	SSZ-13	Seeded	BM* D_1-CHA	20 : 10 : 100 : 1 : 4400	16

*Ball-milled

Experimental

Synthesis of Zeolites

N,N,N-trimethyl-1-adamantammonium hydroxide (TMAdaOH) was provided by SACHEM, Cab-O-Sil M5 was provided by Cabot. The rest of the chemicals were purchased from Sigma-Aldrich. All chemicals were used as received.

The detailed synthetic procedures for the preparation of zeolites with DDR topology (ZSM-58 and Sigma-1) was reported previously by our group.[24, 25]

SSZ-13 (CHA) was synthesized following the work by Zhu *et al.* [26] with some modifications. In a typical procedure, 25% solution of TMAdaOH was mixed with a solution of 0.077 g sodium aluminate and 0.32 g sodium hydroxide in 8.51 g of deionized water. When the solution became clear, 2.78 g of fumed silica Cab-O-Sil M5 and 21.43 g of deionized water were added and kept for aging for 4 h under the stirring. The obtained mixture was transferred to autoclaves and subjected to hydrothermal synthesis at 160 °C for 24 or 120 hours.

After crystallization, zeolites were thoroughly washed with deionized water and dried overnight. These solids were used as starting material for the preparation of seeds *via* ball-milling. The exact procedure can be found elsewhere.[24]

Subsequent syntheses of zeolites with DDR and CHA topology were performed by seed assisted growth using the ball-milled crystals (0.1 wt.% relative to silica source).

The following nomenclature based on synthesis type and framework type code (FTC) was used in the course of the current work: **X – FTC**, where X stands for type of synthesis (D – direct hydrothermal, S – seeded), while FTC is either DDR1 (Sigma-1), DDR2 (ZSM-58) or CHA (SSZ-13). Details on gel composition, synthesis time and nomenclature can be found in Table 1. The as-synthesized crystals were calcined for 10 h at 650 °C and converted to their protonic forms by triple ion-exchange in an aqueous NH_4NO_3 solution (1 M, 80 °C, 2 h, 100 mL per gram of zeolite) followed by calcination at 550 °C.

Fluoride modified S_1-CHA-F was obtained from S_1-CHA following the method described by Xu *et al.* [27] For a typical procedure, 1.2 g of S_1-CHA was dispersed in 20 ml of 0.013M NH_4F solution and left stirring at room temperature until complete evaporation of water (approximately 48 h). The obtained solid was further dried 80°C for 16 h followed by calcination at 600°C for 6 h.

Characterization of Zeolites

The XRD patterns of the powders were recorded in Bragg–Brentano geometry with a Bruker D8 Advance X-ray diffractometer equipped with a LynxEye position-sensitive detector. Measurements were performed at RT by using monochromatic Co$K\alpha$ (λ=1.788970 Å) radiation between 2Θ= 5° and 50°.

Images were recorded using a JEOL JSM-6010LA with a standard beam potential of 10 kV and an Everhart-Thornley detector. X-ray microanalysis (SEM/EDX) confirmed the elemental composition in the sample by scanning microscopy (SEM) coupled with a dispersive X-ray microanalysis system (EDX) with a Silicon-drift detector.

A Malvern Nano ZS zetasizer was used for the analysis of particle size of the wet ball-milled crystals with dynamic light scattering (DLS).

N_2 adsorption was carried out using Tristar II 3020 Micromeritics sorptometer at 77 K. Prior to the experiment samples were outgassed at 350 °C for 16 h.

Temperature-programmed NH_3 desorption (NH_3-TPD) was measured by AutoChem II chemisorption analyzer (Micromeritics). Approximately 0.2 g of the material was first degassed under He flow at 400°C and then saturated with NH_3 at 200 °C during 1 h using a flow of 1.65 % NH_3 in He. The gas mixture was then switched back to He and the sample was purged at 200 °C for about 1 h to remove weakly adsorbed NH_3 molecules. TPD was subsequently recorded under He flow, from 200°C to 800°C. All flow rates were adjusted to 25 mL min^{-1}, and the heating rates were 10°C min^{-1} during different stages of experiment.

Transmission FT-IR spectroscopy was performed using a Nicolet Nexus spectrometer at 4 cm^{-1} resolution equipped with an extended KBr beam splitting and a mercury cadmium telluride (MCT) cryo-detector. The pellets were placed in an IR quartz cell equipped with CaF_2 windows. A movable sample holder allows the sample to be placed in the infrared beam for the measurements or into the furnace for thermal treatments. The cell is connected to a vacuum line for pretreatment. The specimen is activated in vacuum at 400°C for 16 h to remove adsorbed species.

Catalytic Experiments

Dimethyl ether to olefins (DMTO) experiments were performed in a Microactivity Reference unit (PID Eng&Tech) at 400°C and 450°C and ambient pressure. For each experiment, 0.5 g of catalyst (pressed, crushed and sieved to particle sizes 250-420 µm) was placed in a fixed-bed with internal diameter of 9 mm. Conversion, selectivities and yields were calculated on a molar carbon basis. Detailed description of the set-up and calculations can be found elsewhere. [28, 29]

Table 2. Catalytic properties of the zeolites with the DDR topology under the study

Sample	Particle size[a] (μm)	S_{meso}[b] ($m^2\ g^{-1}$)	S_{BET}[c] ($m^2\ g^{-1}$)	V_{micro}[b] ($cm^3\ g^{-1}$)	SiO_2/Al_2O_3[e] (mol mol^{-1})	NH_3 capacity[e] (μmol $NH_3\ g^{-1}$)
D-DDR_1	12-15	20	250	0.10	111	295
S_1-DDR_1	0.4	30	320	0.13	107	306
S_2-DDR_1	5	9	300	0.13	103	318
D-DDR_2	0.5-1.6	22	370	0.14	111	296
S-DDR_2	0.5	17	310	0.13	113	290
D_1-CHA	5-8	7	780	0.30	159	207
D_2-CHA	0.3-1.4	20	770	0.30	168	196
S_1-CHA	0.6-0.7	8	750	0.29	158	208
S_1-CHA-F	0.6-0.7	18	540	0.23	-	-

[a] From SEM images. [b] *t*-plot method applied to the N_2 isotherm. [c] BET method applied to the N_2 isotherm. [e] From NH_3-TPD measurements.

Dimethyl ether (DME) was chosen instead of methanol due to several reasons. Application of DME allowed to achieve very high dilution with nitrogen (DME : N_2= 1 : 19) at the same time avoiding exothermic dehydration of methanol to DME, thus getting rid of heat effects intervention.[29] For a typical experiment, a mixture of 5 mol% of dimethyl ether (DME) in nitrogen was used at a weight-hourly space velocity (*WHSV)* of 1.23 $g_{DME}\ g_{cat}^{-1}\ h^{-1}$. The product mixture was analyzed online with an Interscience CompactGC equipped with a 15 m capillary RTX-1 (1% diphenyl-, 99% dimethylpolysiloxane) column and a flame ionization detector.

Catalytic results are presented as a function of the DME throughput per amount of catalyst used ($g_{DME}\ g_{cat}^{-1}$) and defined as the total amount of DME fed to the catalytic bed before the conversion of DME dropped below 80 %. Selectivities reported in Table 4 are integral values calculated during the active period of the catalyst. The typical evolution of ethylene and propylene selectivities as a function of time is shown in the Supporting Information (Figures S7-S9).

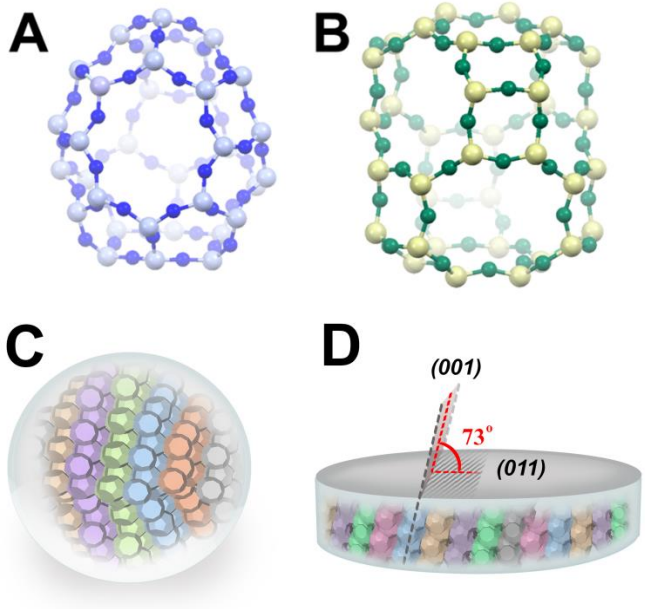

Fig. 1 Cage structures of DDR (A) and CHA (B) frameworks. Arrangement of 8MR-joined 2D pore substructure layers of DDR in (C) spherical and (D) disk-like crystals.

Results and discussion

Results

Characterization of DDR and CHA zeolites

The cage structures of DDR (7.1 × 9.4 Å) and CHA (6.7 × 10.9 Å) are shown in Figure 1. Both topologies belong to the 8-membered ring family (8MR) characterized by large cavities with small window openings. DDR has a 2D porosity, while CHA possesses a 3D pore structure.

Comparison of powder XRD patterns of the synthesized materials with their reference patterns[30] reveals that in all cases the desired topology was obtained and no crystalline impurities could be observed (Figure S1).

Notably, the experimental diffraction pattern of the sample D-DDR_1 shows around 13.3° higher diffraction intensity than expected from the theoretical XRD pattern revealing a preferred orientation of the particles. Consequently, the XRD pattern was subjected to a whole pattern refinement in order to figure out the habit of the crystallites and the direction of their preferred orientation (Figure S2). The refinement results reveal that the D-DDR_1 particles tend to orient preferably along the (011) plane. Moreover, the G_1-factor of 0.023 suggests a platy habit of the crystals, which has been confirmed by scanning electron microscopy. The D-DDR_1 crystals have a disk-like shape and grow preferentially along directions perpendicular to the (0*kl*) crystallographic planes developing a (011) crystal surface. Therefore, the top and bottom surfaces of the D-DDR_1 crystals preferably expose (011) lattice planes along with equivalent (0*kl*) ones, as represented in Figure 1D. These 2D substructures lay in the (001) plane and intersect the top and bottom surfaces of the D-DDR_1 round slabs with inclination angle of 73°, as shown in Figure 1D. Considering this structural arrangement within the crystallite, the diffusion through 8MR channel system is expected to be faster in the disk-like crystals than in spherical particles (Figures 1C and 1D).

Analysis of SEM pictures shows that direct hydrothermal synthesis led to the formation of crystals with disk (Sigma-1),

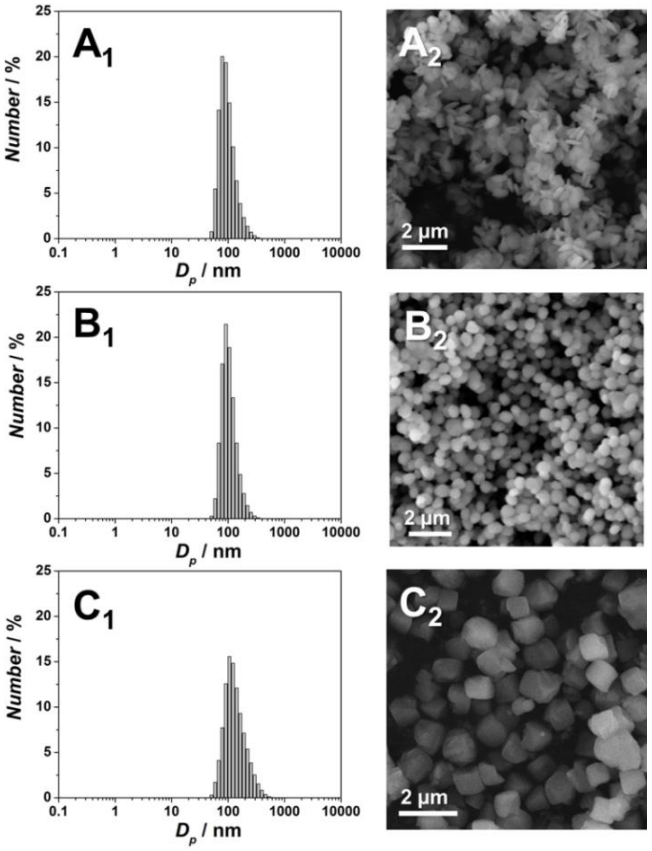

Fig. 2 Particle size distribution of seeds (A_1, B_1, C_1) obtained by DLS, and SEM images of zeolites (A_2, B_2, C_2) obtained from these seeds. A_2 – S_1-DDR$_1$, B_2 – S-DDR$_2$, C_2 – S_1-CHA.

spherical (ZSM-58) and cubic (SSZ-13) shape with relatively broad size distribution (Figure S3, Table 2). On the other hand, seeded growth resulted in the formation of crystals with a narrow size distribution, all particles having similar crystal size (400-600 nm), independently of the topology (Figure 2). DLS analyses of seeding solutions employed for the seeded growth synthesis show that in all cases they contained nanoparticles with an average size of 100 nm. These results suggest that the final crystal size obtained *via* seeded synthesis is more a function of the initial size of seeds than of the zeolite topology. Such interdependence is an indisputable advantage of the seeded growth technique as it allows tuning the particle size.

NH_3-TPD shows that all catalysts possess a similar amount of acid sites independently of the topology and synthesis protocol. For all zeolites, TPD curves are characterized by the presence of one desorption maximum at 410°C (ZSM-58), 450°C (Sigma-1) or 460°C (SSZ-13). The desorption curves of ZSM-58 (D-DDR$_2$ and S_1-DDR$_2$) are also characterized by the presence of a shoulder at 280°C that can be indicative for the presence of weaker acid sites (Figure 3).

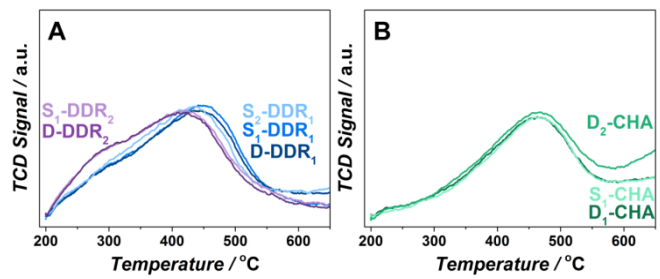

Fig. 3 NH_3-TPD profiles of zeolites with DDR (A) and CHA (B) topology.

Structural differences in the hydroxyl region were investigated by means of IR (Figure 4). The whole spectra can be found in the supporting information (Figure S4). For all samples, the two expected absorbances are always present at 3747 cm^{-1}, characteristic from the ν(OH) of terminal silanols from external surfaces and at 3616 cm^{-1}, associated to the ν(OH) of bridging silanols (Brønsted acid sites).[31]

Table 3. Comparison of catalyst lifetime at different temperatures.

Sample	t_{80} (h)		Throughput (g_{DME} g_{cat}^{-1})		Coke[a] (wt.%)	Coking rate (mg $g_{cat}^{-1}h^{-1}$)
	400 °C	450 °C	400 °C	450 °C		
D-DDR$_1$	0.3	0.7	0.4	0.9	3.2	45.7
S_1-DDR$_1$	1.1	1.6	1.4	2.0	8.8	55.0
S_2-DDR$_1$	0.2	0.4	0.2	0.5	4.3	107.5
D-DDR$_2$	1.3	1.7	1.6	2.1	8.4	49.4
S-DDR$_2$	1.0	1.5	1.2	1.8	9.2	61.3
D_1-CHA	2.6	2.6	3.2	3.2	11.8	45.4
D_2-CHA	4.5	3.6	5.5	4.4	12	33.3
S_1-CHA	3.1	2.0	3.8	2.5	10.5	52.5
S_1-CHA-F	3.5	2.9	4.3	3.6	10.2	35.2

[a] From TGA measurements of deactivated at 450°C catalyst.

For D-DDR$_1$, the band at 3747 cm^{-1} is less prominent, in good agreement with the relatively larger particle size of this sample. Zeolites Sigma-1 synthesized by seeded growth (S_1-DDR$_1$ and S_2-DDR$_1$) display an additional very broad band at 3400 cm^{-1} attributed to silanol nests, progressively increasing from S_1-DDR$_1$ to S_2-DDR$_1$.

These silanol nests, arising from defects in the zeolite framework, represent clusters of silanols interacting *via* medium strength hydrogen bonding. These defects in turn can originate from removal of framework atoms or from incomplete condensation. Interestingly, the spectrum of S_2-DDR$_1$ is characterized by a complex triplet, where, together with the band at 3747 cm^{-1}, two additional vibrations at 3729 and 3706 cm^{-1} are observed. These have been attributed to silanols in different environments but inside the micropores and terminating inner defects. [23, 32] These OHs are slightly more acidic than the band associated with external silanols and are notorious for faster deactivation due to coke retention.[23]

ZSM-58 zeolites display very similar features. For S_1-DDR$_2$ through secondary growth, a broad band is observed with two maxima at 3747 cm^{-1}, 3729 cm^{-1} and additional overlapping bands pointing to multiple inner defects. The band at 3400 cm^{-a1} is also more prominent in comparison with D-DDR$_2$.

Some of the spectra are also characterized by the presence of the band at 3668 cm^{-1} due to the presence of extraframework Al.

The IR spectra obtained from the SSZ-13 samples are rather complex. The Brønsted acidity region is characterized by a triplet with maxima at 3612 cm^{-1}, 3594 cm^{-1} and 3584 cm^{-1}.

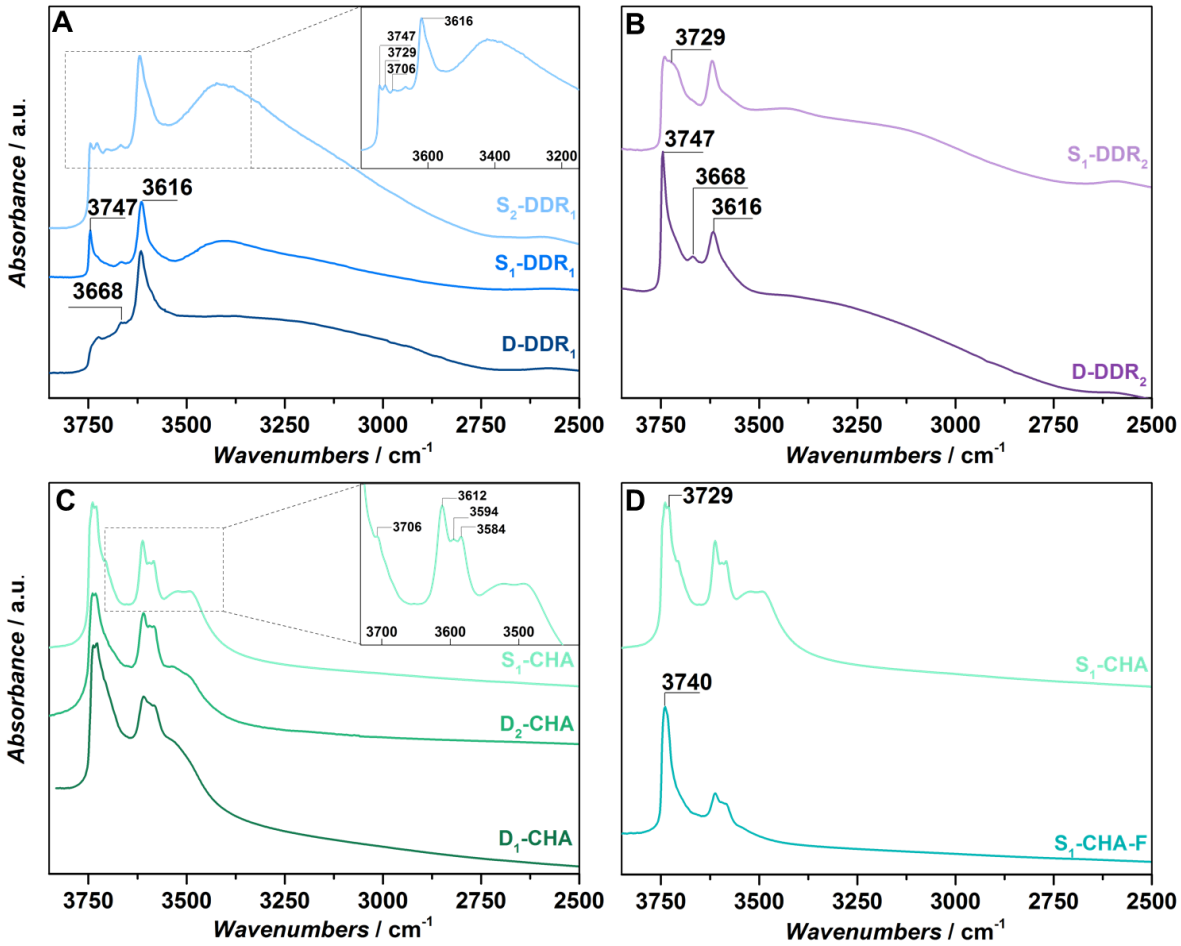

Fig.4 FTIR spectra in the OH-stretching region of activated Sigma-1 (A), ZSM-58 (B), SSZ-13(C) and modified SSZ-13 (D) zeolites.

Bordiga *et al.*[33] identified two bands in SSZ-13 with Si/Al=11.6 at 3616 cm^{-1} and 3584 cm^{-1} and ascribed them to protons of the same strength. The band arising at 3616 cm^{-1} was attributed to the proton located at the 8MR windows while at 3584 cm^{-1} to the proton isolated from the neighbouring cages. The presence of the third peak in our case implies the presence of additional protons in a different geometric position, most likely within the cages. For all samples, silanols are recognised by a doublet at 3740 (isolated silanols) and 3729 cm^{-1} and an additionally appearing band centred at 3706 cm^{-1} for S_1-CHA. Silanol nests are present in all samples as a broad component at around 3520 cm^{-1}, but S_1-CHA is also characterized by a second broad band at around 3490 cm^{-1}. In contrast to parent S_1-CHA, fluoride-modified S_1-CHA-F (Figure 4D) is characterized by a singlet at 3740 cm^{-1} representing isolated silanols, while broad components (3490 and 3520 cm^{-1}) related to silanol nests completely disappear. The ratio of the bands in triplet (3612 cm^{-1}, 3594 cm^{-1} and 3584 cm^{-1}) representing Brønsted acidity seems to remain unchanged, though band absorbance is lower.

Catalytic activity in DMTO

The different zeolites under study were tested in the DMTO reaction. We have recently shown that zeolites with DDR topology have the highest lifetime in MTO reaction at relatively high temperatures (>450°C).[24] In case of SSZ-13, many studies show that, for this topology, milder temperatures (≈400°C) are favourable for longer lifetime.[34] For this reason, two different temperatures (400°C and 450°C) were selected to allow for a meaningful comparison. Figure 5 and Table 3 show the obtained lifetimes and related throughput, while conversion as a function of time is presented in the Supporting Information file (Figure S6). In line with previous papers dedicated to Sigma-1 and ZSM-58,[24, 25] zeolites with DDR topology display an up to twice higher throughput at 450°C in comparison with 400°C. The fast deactivation of DDR zeolites at 400°C was attributed to the formation of diamondoid species remaining in the zeolite cages and in contrast to methylbenzenes not reacting further with methanol.[24]

Interestingly, there is no direct correlation between catalyst lifetime and particle size. Large crystals (10-15 µm) of directly synthesized D-DDR_1 show longer lifetimes than much smaller S_2-DDR_1 at 450°C (Table 3, 0.9 *vs* 0.5 g_{DME} g_{cat}^{-1}). Accordingly, the nanosized S-DDR_2 with multiple internal defects displays

Table 4. Product selectivities obtained in DMTO reaction over zeolites under study at 400°C and 450°C.

Sample	Selectivity, %									
	C1-C4[a]		C2[=a]		C3[=a]		C4[=a]		C5-6[a]	
	400°C	450°C	400°C	450°C	400°C	450°C	400°C	450°C	400°C	450°C
D-DDR$_1$	3	2	37	42	39	32	7	7	1	1
S$_1$-DDR$_1$	5	2	25	38	47	43	15	13	2	2
S$_2$-DDR$_1$	1	2	22	32	45	42	10	10	1	1
D-DDR$_2$	4	3	23	39	48	41	15	11	2	2
S-DDR$_2$	2	2	21	32	45	44	13	12	5	5
D$_1$-CHA	7	4	42	50	35	31	12	10	5	5
D$_2$-CHA	4	3	47	55	33	28	11	9	6	5
S$_1$-CHA	6	3	40	51	37	32	13	10	4	4
S$_1$-CHA-F	4	3	41	51	37	31	12	9	6	6

[a] Integral values calculated during the active period of the catalyst.

slightly worse performance than its micrometer hydrothermally synthesized counterpart D-DDR$_2$. To demonstrate that the observed relation is not topology dependent, the catalytic behaviour of SSZ-13 was also investigated. First of all, in contrast to Sigma-1 and ZSM-58, SSZ-13, except D$_1$-CHA, show longer lifetimes at 400°C. However, even at 450°C there is a noticeable difference in lifetimes for DDR and CHA in favour of CHA. Such a prolonged lifetime of these catalysts is explained on the basis of the bigger dimensions and particular shape of the main CHA cage, which is able to accumulate more aromatics and is believed to stabilize "hydrocarbon pool" species.[35-37] Furthermore, there is a higher probability of blocking the 2D pore network of ZSM-58 and Sigma-1 than the 3D porosity of SSZ-13, leading to a faster deactivation of DDR. According to the literature,[38] the diamondoid species can be also formed in CHA cage however below 300°C leading to the prompt deactivation as in case of DDR. Thus the different optimum temperatures for DDR (450°C) and CHA (400°C) can be related to the nature of active species formed at these temperatures and their participation either in aromatic cycle or coke formation. In turn, the formation of different aromatic species is defined by cage architecture, location and strength of the acid site.

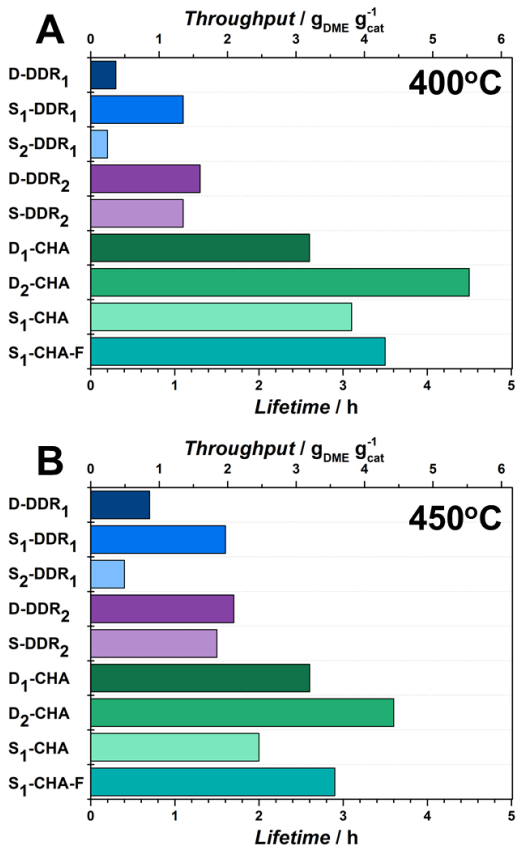

Fig. 5 Catalytic activity of zeolites under study at 400°C (A) and 450°C (B) in DMTO reaction.

The highest DME throughput (5.5 g$_{DME}$ g$_{cat}^{-1}$) is observed for D$_2$-CHA at 400°C followed by S$_1$-CHA (3.8 g$_{DME}$ g$_{cat}^{-1}$). It is obvious that, despite minor differences in size and acidity, noticeable differences are found in DME throughputs. Moreover, D$_1$-CHA, whose lifetime seems to be temperature independent, outperforms S$_1$-CHA at 450°C, clearly showing that the quality of the crystal is more important than its size. Fluoride modification seems to have positive effect on catalyst lifetime as it results in higher DME throughput for S$_1$-CHA-F in comparison with S$_1$-CHA, which is especially noticeable at 450°C (3.6 *vs* 2.5 g$_{DME}$ g$_{cat}^{-1}$).

To summarize, an important tendency is found: zeolites prepared by seeded growth deactivate faster than directly synthesized zeolites. As the only substantial difference between these zeolites is the presence of internal silanols and silanol nests, faster deactivation is attributed to the presence of these features.[23]

Product Selectivities

Product selectivities observed at 400°C and 450°C in DMTO are shown in Table 4. Ethylene, propylene and butenes are the main products for both DDR and CHA topologies with some presence of higher hydrocarbons and paraffins. The amount of paraffins and higher hydrocarbons is especially noticeable for CHA catalyst (up to 10%), which has larger dimensions of cage and pore openings. For DDR zeolites, higher hydrocarbons are mostly formed on the external surface as they cannot pass the window opening. Independently on topology, higher temperatures lead to higher selectivities to ethylene and lower selectivities to propylene and butenes as a result of kinetic competition between the aromatic and olefinic cycle.[24] The maximum selectivity of ethylene for all catalysts under study (Figures S7 – S9) coincides with the breakthrough of DME as a result of accumulation methylbenzenes and polycondensed methylated species, responsible not only for ethylene formation but also for deactivation.[39] Moreover, under the same conditions, the amount of produced ethylene on CHA catalysts is at least 10 % higher than for Sigma-1 and ZSM-58. It is also important to mention that for DDR catalysts, due to very short lifetime and high rate of coking, the carbon balance is not always completely closed. Especially, D-DDR_1, S_2-DDR_1 at 400°C exhibit high selectivities towards coke formation (> 10%).

Though the method of zeolite preparation (direct *vs* seeded) has a noticeable effect on catalyst lifetime, there is no pronounced relation between product distribution and method of preparation.

Discussion

Seeding was shown to be an appropriate way to significantly reduce synthesis time and a tool to control the particle size, which makes it very attractive from large-scale application perspective. Recently Mintova *et al*. [40] examined some common issues of zeolite crystal growth, including nucleation *via* seeding. Among the advantages of seeded growth authors also listed reduced formation of undesired phase and fast nuclei formation. Obviously, the weak point is that seeded growth approach can often lead to aggregation and intergrown crystals.[41, 42] This aggregation seems to be correlated with the amount of seeds used. As zeolites in this work were synthesized with very low amount of seeds (0.1% wt.), neither aggregation nor intergrowth was observed.

Valtchev *et al.* fairly mentioned that, although the seeded method is already widely used, the mechanism is barely known. [42] However, the way this can be achieved is still a matter of discussion. Xiao *et al*. demonstrated that zeolites crystallize on the surface of seeds *i.e.* forming core-shell structures.[21, 43] The crystal growth proceeds on partially dissolved seeds in alkaline media, but without dissolution to primary building blocks. An attempt to crystallize zeolite BEA only in the presence of primary building blocks resulted in an amorphous phase.[21] On the other hand, Okubo *et al*. suggest that seeds are disaggregated into much smaller subunits that, in turn, provide surface for crystal growth, *i.e.* again through partial dissolution, however, herein building units play the key factor. [44] Authors showed further that it is possible to synthesize zeolites using seeds of other topology, which have common building units. The mechanisms proposed by Xiao *et al*. [21, 43] and Okubo *et al*. [20] for the SDA-free synthesis of zeolites, in principle, hold well for this work . However, considering the very small amount of seeds used for zeolite synthesis in this work, we tentatively suggest that dissolution of seeds proceeds to much smaller aggregates in comparison to previously mentioned works, giving rise to nuclei which act as a core to build new zeolite crystals. With this little amount of seeds, application of SDA is necessary. The size of the formed nuclei would then depend on the initial size of the seeds and determine the final crystal size. Thus, the 100 nm seeds led to formation of crystals with particle size < 500 nm. If the latter are used as seeds these crystals result in the formation of 2.5 µm particle, 2,5 µm seeds will form 5 µm and so on.

Considering that build-up of the crystal starts not from the elementary building unit but already from the pre-formed core, the formation of a framework with T-site vacancies can be anticipated. From this perspective, the secondary growth of building units can be compared - to a certain degree - with random Tetris® blocks which are not always matching the surface and thus leaving some “gaps” in crystal structure. These “gaps” or T-vacancies are saturated with protons from the nearest oxygens giving rise to the hydroxyl nests and/or other silanol defects.[45] Moreover, during the hydrothermal synthesis, T-vacancies present in seeds are not healed under synthesis conditions and are progressively accumulating in the newly synthesised zeolite crystal. For example, in case of S_2-DDR_1, the core part of the crystal is represented by much bigger fragments of partially dissolved seeds that already possess T-vacancies (as it was also synthesized by seed-assisted method). Thus, the observed increased amount of silanol nests is a consequence of defects accumulation.

The term *hydroxyl nest* represents the defect where a SiO_4 or AlO_4 tetrahedron is replaced with four hydroxyls. The structural defect can also exist in the form of *geminal* silanols $=Si(OH)_2$ or bridged *vicinal* silanols. It is important to mention that the defects seen *via* spectroscopic tools (NMR and FTIR mainly) are only the tip of the iceberg, as the majority of them cannot be observed directly. This is the consequence of continuous transformation of structural defects due to dihydroxylation, dehydration or deprotonation happening already at room temperature. The dynamic behaviour of these defects causes drastic changes in characteristic signals obtained by NMR and FTIR. [45]

In general, there are many possible reasons leading to the formation of defects, dealumination being the most common but not the only one. [10] Fernandez et al. [46] have shown that formation and location of silanol defects can be governed by the SDA during zeolite crystallization. In this case, defects are located in close proximity to the template. In this work, we highlight another origin of defects coming from a mismatching crystal growth.[45]

The catalytic testing of synthesized zeolites in DMTO reaction revealed that zeolites prepared by seeded growth deactivate

much faster than directly hydrothermally synthesized materials. In our previous work, we have already extensively discussed influence of defects on prominently deactivating Sigma-1 in the MTO reaction.[24] In addition, due to the preferential orientation of lattice planes with an inclination angle of 73^{o} to the disk (Figure 1D), the diffusion pathway for Sigma-1 is defined by the thickness of the crystal (≈100 nm for S_1-DDR$_1$). This dimension is at least 5 times smaller than for defect-free spherical D-DDR$_2$. Despite such five-fold shorter diffusion pathway in case of S_1-DDR$_1$, these catalysts show slightly shorter lifetime in DMTO reaction (Figure 5), again highlighting the importance of crystal quality. This observation highlights that effect coming from structural defects overweighs crystal size effect. The increased amount of defects facilitates formation of internal coke, significantly affecting the rate of deactivation. This relationship between defects and catalyst deactivation is already a well-established feature explained by the so called "retention effect" of coke species.[23, 47] Sazama *et al.* showed that defective sites in ZSM-5 facilitate hydrogen transfer reactions thus producing higher amount of paraffins and aromatics and leading to twice faster deactivation.[48] On the other hand, faster crystal growth kinetics in the presence of seeds, might also lead to different distribution of Al in the zeolite framework in comparison to zeolites synthesized by direct hydrothermal growth, thus affecting catalytic performance. [49] There are many parameters affecting Al distribution like pH, SDA, precursors and synthesis conditions.[50] According to Dedecek, "*the greater heterogeneity of mixtures results finally in higher population of Al pairs and vice versa rather homogeneous up to clear up solutions lead to higher population of single Al atoms*."[50] Adapted to our case, there is a higher probability of Al-zoning for catalysts prepared by seeding as a consequence of starting from heterogeneous seed-containing synthesis solution. Formation of Al-rich regions in turn can lead to higher coking rates due to higher probability of olefins from the two nearest sites to form aromatics. [47, 51] This effect should be further explored.

The comparison of selectivities obtained for defective and non-defective zeolites in this work does not reveal significant difference in product distribution. Logically, for 8MR zeolites, selectivities are rather governed by the cage and window dimensions.[35-37] On the other hand, enhanced hydrogen transfer reactions would speed up coke formation rate. Indeed, the analysis of coking rate (Table 3) expressed as the mass of coke formed during the active period shows that rate of coke formation is almost twice higher for seeded zeolites than for hydrothermally synthesized ones (compare D-DDR$_1$ *vs* S_2-DDR$_1$ and D$_2$-CHA *vs* S_1-CHA).

The results obtained in this work highlight the importance of crystal quality, which turns out to be more important than particle size. Though seeded growth approach allows tuning crystal size on demand and significantly reduces synthesis time, its negative impact on DMTO (MTO, MTH, MTG) catalysis outweighs all listed advantages. Further optimization of zeolite synthetic procedures based on secondary growth approach is required. From this perspective, synthesis of zeolites in fluoride media is rather promising. It has been shown that with the assistance of fluoride, synthesized crystals possess less defects,[52] while post-synthetic treatment with FeF_3/NH_4HF_2 selectively removes internal silanols from synthesized zeolites improving catalyst lifetime by a factor of ten.[53] Valtchev *et al.* compared synthesis of nano-ZSM-5 by seed assisted method in OH^- and F^- media, the latter possessing significantly less structural defects.[54] In this work, the post-synthetic fluoride treatment with NH_4F was chosen as a tool to heal defects in zeolite crystals. IR results clearly demonstrated that such treatment led to selective removal of silanol nests and internal silanols from zeolite crystal. Unlike for ZSM-5, fluoride treatment did not lead to the generation of mesopores in SSZ-13, however led to a noticeable surface area loss. Despite this loss in surface area (≈30%) and micropore volume (≈20%), S_1-CHA-F showed longer lifetimes in DMTO reaction and lower coking rates. One has to be aware that concentration of NH_4F had to be thoroughly optimized as further increase in F^- concentration led to removal of Brønsted acid sites from the zeolite framework (Figure S5).

Herein, we have further confirmed the negative impact of defects arising from seeded growth on DMTO performance. It is also important to mention that there are a number of reactions that are catalysed solely by defects. Abate *et al.* dedicated a paragraph in the recent perspective about the role of defects in such reactions like Beckmann rearrangement, etherification of 5-hydroxymethylfurfural (HMF) to produce, for instance, biodiesel components.[10] Thus, the seeding method to produce defective zeolites can be beneficial for future applications in reactions catalysed by hydroxyl nests.

Conclusions

Zeolites with DDR (Sigma-1 and ZSM-58) and CHA (SSZ-13) topology were synthesized by direct hydrothermal synthesis and seed assisted method. Synthesized zeolites appeared to have similar amount of Brønsted acid sites. However, zeolites prepared by seeded growth contain a significant amount of internal silanols and hydroxyl nests due to the fast crystal growth kinetics. These multiple defects have a negative impact on catalytic performance in the DMTO reaction in terms of lifetime, but did not affect product distribution. Such deactivation behaviour is a consequence of the silanols participating in hydrogen transfer reactions and thus speeding up coke formation rate. These silanols can be selectively removed from by treatment with NH_4F. All zeolites under study exhibited high selectivities to ethylene, propylene and butenes (>90%), selectivities being dependent on reaction temperature ($\uparrow T \rightarrow \uparrow S_{2=}$, $\downarrow SC_{3=}\text{-}C_{4=}$) and size of cage ($\uparrow$size $\rightarrow \uparrow S_{2=}$, $\downarrow SC_{3=}\text{-}C_{4=}$).

Acknowledgements

This research received funding from the Netherlands Organisation for Scientific Research (NWO) in the framework of the TASC Technology Area "Syngas, a Switch to Flexible New Feedstock for the Chemical Industry (TA-Syngas)".

Notes and references

1. J. Weitkamp, *Solid State Ionics*, 2000, **131**, 175-188.
2. S. B. Wang and Y. L. Peng, *Chem. Eng. J.*, 2010, **156**, 11-24.
3. N. Kosinov, J. Gascon, F. Kapteijn and E. J. M. Hensen, *J. Membr. Sci.*, 2016, **499**, 65-79.
4. E. E. McLeary, J. C. Jansen and F. Kapteijn, *Microporous Mesoporous Mater.*, 2006, **90**, 198-220.
5. J. Gascon, F. Kapteijn, B. Zornoza, V. Sebastian, C. Casado and J. Coronas, *Chem. Mater.*, 2012, **24**, 2829-2844.
6. A. Corma, *J. Catal.*, 2003, **216**, 298-312.
7. K. Tanabe and W. F. Holderich, *Appl.Catal., A*, 1999, **181**, 399-434.
8. A. Corma, L. T. Nemeth, M. Renz and S. Valencia, *Nature*, 2001, **412**, 423-425.
9. J. D. Lewis, S. Van de Vyver and Y. Roman-Leshkov, *Angew. Chem. Int. Ed.*, 2015, **54**, 9835-9838.
10. S. Abate, K. Barbera, G. Centi, P. Lanzafame and S. Perathoner, *Cat. Sci. Tech.*, 2016, **6**, 2485-2501.
11. H. Bekkum and H. W. Kouwenhoven, *Zeolite Manual for the Organic Chemist*, 2012.
12. A. M. Beale, F. Gao, I. Lezcano-Gonzalez, C. H. F. Peden and J. Szanyi, *Chem. Soc. Rev.*, 2015, **44**, 7371-7405.
13. J. Gascon, J. R. van Ommen, J. A. Moulijn and F. Kapteijn, *Cat. Sci. Tech.*, 2015, **5**, 807-817.
14. C. Gücüyener, J. van den Bergh, A. M. Joaristi, P. Magusin, E. J. M. Hensen, J. Gascon and F. Kapteijn, *J. Mater. Chem.*, 2011, **21**, 18386-18397.
15. J. Gascon, W. Blom, A. van Miltenburg, A. Ferreira, R. Berger and F. Kapteijn, *Microporous Mesoporous Mater.*, 2008, **115**, 585-593.
16. C. Liu, L. Bai, J. M. Zhang, D. Hu, M. Li, G. F. Zeng, Y. F. Zhang, W. Wei and Y. H. Sun, *Microporous Mesoporous Mater.*, 2016, **225**, 312-322.
17. M. Moliner, C. Martinez and A. Corma, *Chem. Mater.*, 2014, **26**, 246-258.
18. Q. M. Wu, X. Wang, G. D. Qi, Q. Guo, S. X. Pan, X. J. Meng, J. Xu, F. Deng, F. T. Fan, Z. C. Feng, C. Li, S. Maurer, U. Muller and F. S. Xiao, *J. Am. Chem. Soc.*, 2014, **136**, 4019-4025.
19. Q. Sun, N. Wang, G. Guo and J. Yu, *Chem. Commun.*, 2015, **51**, 16397-16400.
20. Y. Kamimura, S. Tanahashi, K. Itabashi, A. Sugawara, T. Wakihara, A. Shimojima and T. Okubo, *J. Phys. Chem. C*, 2011, **115**, 744-750.
21. B. Xie, H. Y. Zhang, C. G. Yang, S. Y. Liu, L. M. Ren, L. Zhang, X. J. Meng, B. Yilmaz, U. Muller and F. S. Xiao, *Chem. Commun.*, 2011, **47**, 3945-3947.
22. R. Martinez-Franco, Z. Li, J. Martinez-Triguero, M. Moliner and A. Corma, *Cat. Sci. Tech.*, 2016, **6**, 2796-2806.
23. K. Barbera, F. Bonino, S. Bordiga, T. V. W. Janssens and P. Beato, *J. Catal.*, 2011, **280**, 196-205.
24. I. Yarulina, J. Goetze, C. Gücüyener, L. van Thiel, A. Dikhtiarenko, J. Ruiz-Martinez, B. M. Weckhuysen, J. Gascon and F. Kapteijn, *Cat. Sci. Tech.*, 2016, **6**, 2663-2678.
25. Y. Kumita, J. Gascon, E. Stavitski, J. A. Moulijn and F. Kapteijn, *Appl.Catal., A*, 2011, **391**, 234-243.
26. Q. J. Zhu, J. N. Kondo, R. Ohnuma, Y. Kubota, M. Yamaguchi and T. Tatsumi, *Microporous Mesoporous Mater.*, 2008, **112**, 153-161.
27. T. Xu, Q. Zhang, H. Song and Y. Wang, *J. Catal.*, 2012, **295**, 232-241.
28. I. Yarulina, S. Bailleul, A. Pustovarenko, J. R. Martinez, K. D. Wispelaere, J. Hajek, B. M. Weckhuysen, K. Houben, M. Baldus, V. Van Speybroeck, F. Kapteijn and J. Gascon, *ChemCatChem*, 2016, **8**, 3057-3063.
29. I. Yarulina, F. Kapteijn and J. Gascon, *Cat. Sci. Tech.*, 2016, **6**, 5320-5325.
30. C. Baerlocher, L. B. McCusker and D. H. Olson, *Atlas of Zeolite Framework Types*, Elsevier Science, 2007.
31. S. Bordiga, P. Ugliengo, A. Damin, C. Lamberti, G. Spoto, A. Zecchina, G. Spano, R. Buzzoni, L. Dalloro and F. Rivetti, *Top. Catal.*, 2001, **15**, 43-52.
32. F. Thibault-Starzyk, A. Vimont and J. P. Gilson, *Catal. Today*, 2001, **70**, 227-241.
33. S. Bordiga, L. Regli, D. Cocina, C. Lamberti, M. Bjorgen and K. P. Lillerud, *J. Phys. Chem. B*, 2005, **109**, 2779-2784.
34. F. Bleken, M. Bjorgen, L. Palumbo, S. Bordiga, S. Svelle, K. P. Lillerud and U. Olsbye, *Top. Catal.*, 2009, **52**, 218-228.
35. Y. Bhawe, M. Moliner-Marin, J. D. Lunn, Y. Liu, A. Malek and M. Davis, *ACS Catal.*, 2012, **2**, 2490-2495.
36. J. W. Park, J. Y. Lee, K. S. Kim, S. B. Hong and G. Seo, *Appl.Catal., A*, 2008, **339**, 36-44.
37. J. Z. Li, Y. X. Wei, J. R. Chen, S. T. Xu, P. Tian, X. F. Yang, B. Li, J. B. Wang and Z. M. Liu, *ACS Catal.*, 2015, **5**, 661-665.
38. J. R. Chen, J. Z. Li, Y. X. Wei, C. Y. Yuan, B. Li, S. T. Xu, Y. Zhou, J. B. Wang, M. Z. Zhang and Z. M. Liu, *Catal. Commun.*, 2014, **46**, 36-40.
39. E. Borodina, F. Meirer, I. Lezcano-Gonzalez, M. Mokhtar, A. M. Asiri, S. A. Al-Thabaiti, S. N. Basahel, J. Ruiz-Martinez and B. M. Weckhuysen, *ACS Catal.*, 2015, **5**, 992-1003.
40. J. Grand, H. Awala and S. Mintova, *CrystEngComm*, 2016, **18**, 650-664.
41. N. Ren, J. Bronic, B. Subotic, X. C. Lv, Z. J. Yang and Y. Tang, *Microporous Mesoporous Mater.*, 2011, **139**, 197-206.
42. G. Majano, A. Darwiche, S. Mintova and V. Valtchev, *Ind. Eng. Chem. Res.*, 2009, **48**, 7084-7091.
43. B. Xie, J. Song, L. Ren, Y. Ji, J. Li and F.-S. Xiao, *Chem. Mater.*, 2008, **20**, 4533-4535.
44. K. Itabashi, Y. Kamimura, K. Iyoki, A. Shimojima and T. Okubo, *J. Am. Chem. Soc.*, 2012, **134**, 11542-11549.
45. A. A. Sokol, C. R. A. Catlow, J. M. Garces and A. Kuperman, *J. Phys. Chem. B*, 2002, **106**, 6163-6177.
46. E. Dib, J. Grand, S. Mintova and C. Fernandez, *Chem. Mater.*, 2015, **27**, 7577-7579.
47. U. Olsbye, S. Svelle, M. Bjorgen, P. Beato, T. V. W. Janssens, F. Joensen, S. Bordiga and K. P. Lillerud, *Angew. Chem. Int. Ed.*, 2012, **51**, 5810-5831.
48. P. Sazama, B. Wichterlova, J. Dedecek, Z. Tvaruzkova, Z. Musilova, L. Palumbo, S. Sklenak and O. Gonsiorova, *Microporous Mesoporous Mater.*, 2011, **143**, 87-96.
49. N. Danilina, F. Krumeich, S. A. Castelanelli and J. A. van Bokhoven, *J. Phys. Chem. C*, 2010, **114**, 6640-6645.
50. J. Dedecek, Z. Sobalik and B. Wichterlova, *Catal. Rev. Sci. Eng.*, 2012, **54**, 135-223.
51. T. Liang, J. Chen, Z. Qin, J. Li, P. Wang, S. Wang, G. Wang, M. Dong, W. Fan and J. Wang, *ACS Catal.*, 2016, **6**, 7311-7325.
52. P. Tian, Y. X. Wei, M. Ye and Z. M. Liu, *ACS Catal.*, 2015, **5**, 1922-1938.

53. M. R. Li, Y. P. Zhou, C. Ju and Y. M. Fang, *Appl.Catal., A*, 2016, **512**, 1-8.
54. Z. X. Qin, L. Lakiss, L. Tosheva, J. P. Gilson, A. Vicente, C. Fernandez and V. Valtchev, *Adv. Funct. Mater.*, 2014, **24**, 257-264.

